American Journal of Energy Engineering
2025, Vol. 13, No. 2, pp. 54-66
https://doi.org/10.11648/j.ajee.20251302.12

Research Article

Numerical Simulation of Tee Pipe Failure Under Mixed Mode-I/III Loading

Lu Wang[1, 2], Yujun Xie[1, *], Kaile Wang[1], Yihan Kang[1], Bingxue Wang[1], Yuqing Du[1]

[1]College of Petroleum Engineering, Liaoning Petrochemical University, Fushun, China

[2]College of Pipeline and Civil Engineering, China University of Petroleum (East China), Qingdao, China

Abstract

This study probes the brittle fracture mechanisms of an S32205 duplex stainless steel tee pipe (DN300×10 mm) subjected to mixed-mode I/III loading under internal pressures spanning 10 to 30 MPa, leveraging advanced finite element analysis to address reliability concerns in high-pressure oil and gas transport systems. Drawing on recent fracture mechanics insights, an energy-driven three-dimensional framework was formulated to forecast crack propagation, emphasizing metallurgical flaws such as micro-cracks and σ-phase precipitates across varied pressure conditions. By partitioning the crack tip into discrete zones, the model calculates energy release rates and stress intensity factors (K_I, K_{III}, K_{eff}) for crack morphologies, including trifurcation, symmetric branching, and lateral bifurcation. Findings reveal that Mode I stresses maximize at the crack's deepest point (90°), with K_I and K_{eff} exhibiting nonlinear escalation as pressure, crack depth-to-length ratio (a/c), and crack half-length (c) increase, portending elevated risks of unstable crack advancement. Mode III stresses, peaking at 60° and 120°, induce localized tearing, with K_{III} displaying marked sensitivity to pressure fluctuations. Pressure-amplified stress concentrations at the branch neck and main pipe abdomen corroborate chevron fracture patterns observed in duplex stainless steel tests, affirming the model's fidelity. The results elucidate the synergistic degradation of fracture toughness by micro-cracks, σ-phase, and pressure-induced stresses, precipitating brittle failure. Heat treatment at 1030°C with water quenching to mitigate σ-phase and periodic ultrasonic inspections are advocated to bolster tee pipe durability in rigorous oilfield settings.

Keywords

Tee Pipe Failure, Mixed-mode I/III Loading, Brittle Fracture, S32205 Duplex Stainless Steel, Energy-based Model, Stress Intensity Factor

1. Introduction

Tee pipe fittings fulfill an essential function in connecting and diverting flows within subsea oil and gas pipelines, long-distance transmission systems, and gathering networks [1, 2]. However, geometric complexities at the branch-main pipe junction render tee fittings prone to brittle fracture under harsh operating environments [3, 4]. With the increasing adoption of high-pressure and large-diameter pipelines, tee failure has emerged as a critical challenge, necessitating a

*Corresponding author: yjxiefs@qq.com (Yujun Xie)

Received: 8 May 2025; **Accepted:** 3 June 2025; **Published:** 11 June 2025

thorough exploration of its underlying mechanisms.

A notable case involved an S32205 duplex stainless steel tee pipe that experienced catastrophic failure during a 22 MPa hydraulic test, exhibiting brittle fracture characteristics [5]. Analysis revealed compromised mechanical properties, including reduced elongation, excessive hardness, and minimal Charpy impact toughness, reflecting pronounced brittleness. Fractures, initiating at high-stress regions in the branch neck and main pipe belly, were driven by metallurgical defects, such as microcracks and σ phase precipitation.

To address such complex fractures, a three-dimensional energy-based model under mixed Mode I/III loading employs a novel partitioning of the crack tip into four subregions, effectively capturing diverse fracture configurations, including trifurcation, symmetrical branching, and lateral bifurcation [6]. Unlike traditional fracture criteria limited to single crack initiation, this model quantifies energy release rates ($G_{\max}$) and effective fracture toughness (K_{eff-C}), offering deeper insights into multiple crack propagation [6].

This study advances the application of this model through finite element simulations of tee pipe crack propagation, quantifying the role of metallurgical defects in brittle fracture, and offering critical insights for the safe design of oil and gas transportation infrastructure.

2. Theoretical Framework

Accurate prediction of crack propagation under mixed-mode loading hinges on robust fracture criteria [7]. However, established fracture models, such as criteria based on maximum tangential stress and strain energy density, are primarily effective for initial crack propagation under single-mode loading [8-10]. These models are ill-equipped to address complex fracture configurations, such as branching or kinking, particularly in mixed-mode scenarios critical to tee pipe failures [11-17].

The energy-based model by Wang et al. (2023) is well-suited to analyzing mixed Mode I/III loading, aptly suited to the intricate fracture patterns inherent in tee pipe junctions driven by geometric discontinuities [6]. By segmenting the crack tip into distinct zones (A_1 to A_4), the model precisely computes J_i -integrals to predict complex fracture modes, such as trifurcation, precisely determining crack growth trajectories. Unlike conventional Mode I models focused on opening-mode cracks, this model accounts for the interaction between shear and tensile stresses, markedly improving predictive reliability in brittle regions affected by metallurgical defects, as observed in tee pipe failures [5].

2.1. Overview of the Energy-Based Model

Multiple crack initiation within the K-dominant region is critical for fracture prediction. This process may be modeled as crack fronts reorienting in diverse directions. In crack front reorientation under mixed-mode fracture, the fracture driving force is expressed as detailed in [18-23].

$$G = \lim_{A\to 0} \iint_{A} we_i n_i d\Omega, \tag{1}$$

where $e_i = \cos\alpha_i$ and α_i is the angle between shifting direction of the boundary and x_i -axis; n_i is the unit normal vector of the boundary [23, 24].

For a mixed Mode-I/III crack, there are five basic potential fracture configurations, i.e., the crack tri-branching as shown in Figure 1, side-branching as shown in Figure 2, symmetrical branching as shown in Figure 3, kinking as shown in Figure 4 and extension as shown in as shown in Figure 5. The concerned energy release rate of each potential fracture configuration can be given by

$$G_{\max} = \frac{\left(1-\mu^2\right)\left(K_I^2 + K_{III}^2/(1-\mu)\right)}{E}\cdot\Gamma(\varphi) \tag{2}$$

where $\Gamma(\varphi)$, a normalized energy-driven parameter, governs the propagation of various fracture configurations.

where φ, denotes the mode mixity angle，a normalized parameter, represents the proportional influence of stress intensity factors K_I and K_{III} in mixed-mode loading can be given by

$$\varphi = \frac{2}{\pi}\arctan\frac{K_I}{K_{III}/\sqrt{1-\mu}} \tag{3}$$

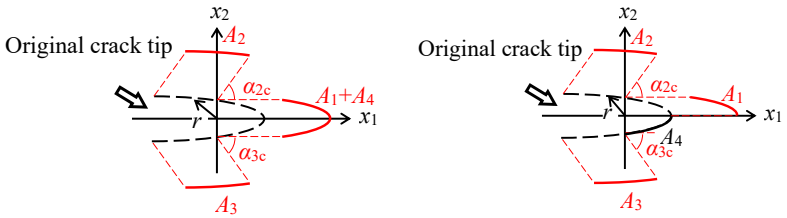

(a) Form 1 (b) Form 2

Figure 1. *Geometrical Sketch of crack tri-branching Initiation from a Mixed-Mode I/III Crack Tip.*

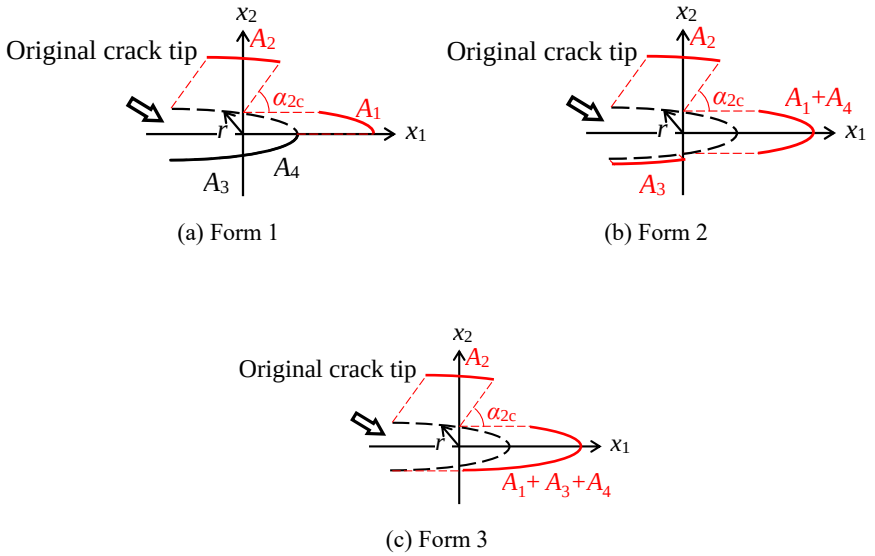

(a) Form 1 (b) Form 2

(c) Form 3

Figure 2. *Geometrical Sketch of crack side-branching Initiation from a Mixed-Mode I/III Crack Tip.*

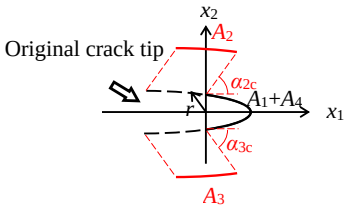

Figure 3. *Geometrical Sketch of crack symmetrical branching Initiation from a Mixed-Mode I/III Crack Tip.*

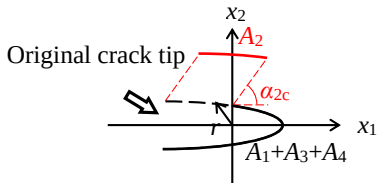

Figure 4. *Geometrical Sketch of crack kinking Initiation from a Mixed-Mode I/III Crack Tip.*

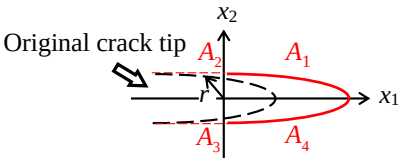

Figure 5. *Geometrical Sketch of crack extension Initiation from a Mixed-Mode I/III Crack Tip.*

In brittle materials under mixed-mode loading, the Griffith criterion [25, 26]. posits that crack propagation commences once the fracture driving energy $G_{\max}$ attains its critical threshold G_C, i.e.,

$$G_{\max} = G_C . \tag{4}$$

For Mode I fracture behavior in tee pipe structures, when the energy release threshold $G_{\max} = G_C$, this implies

$$G_C = \frac{\left(1-\mu^2\right)K_{IC}^2}{E} \tag{5}$$

Where μ denotes Poisson's ratio, K_{IC} the Mode I fracture toughness, and E the modulus of elasticity.

The effective stress intensity factor is characterized as

$$K_{eff} = \sqrt{K_I^2 + K_{III}^2 / (1-\mu)} \tag{6}$$

for tee pipe junctions under mixed-mode loading. Additionally, the *K*-based criterion for mixed-mode I/III fractures across diverse fracture patterns is established as

$$K_{eff} = K_{eff-C} = \eta \cdot K_{IC} \tag{7}$$

where K_{eff-C} represents critical effective stress intensity factor, η is a dimensionless factor, termed the configuration-dependent fracture toughness amplification factor, which is influenced by the crack geometry, such as tri-branching, side-branching, symmetrical-branching, kinking, extension, and the mode mixity angle φ, with values of η for diverse crack Configurations prese0nted in Table 1.

Table 1. Fracture Toughness Amplification Factor η for Mixed-Mode I/III Cracks across Various Configurations.

Fracture configuration		η
crack tri-branching (Figure 1)	Form 1.	$\frac{2}{\left[1+\left(4/\pi^2\right)\sin^4\left(\pi\varphi/2\right)\right]^{1/4}}$
	Form 2.	2
crack side-branching (Figure 2)	Form 1.	2
	Form 2.	$\frac{2}{\left[1+\left(4/\pi^2\right)\sin^4\left(\pi\varphi/2\right)\right]^{1/4}}$
	Form 3.	$\frac{2}{\left[1+\left(4/\pi^2\right)\sin^4\left(\pi\varphi/2\right)\right]^{1/4}}$
crack symmetrical branching (Figure 3)		$\frac{2}{\left[1+\left(4/\pi^2\right)\sin^4\left(\pi\varphi/2\right)\right]^{1/4}}$
crack kinking (Figure 4)		$\frac{2}{\left[1+\left(4/\pi^2\right)\sin^4\left(\pi\varphi/2\right)\right]^{1/4}}$
crack extension (Figure 5)	Form 1. (A=A1+A2+A3+A4)	1
	Form 2. (A=A1)	2
	Form 3. (A=A1+A4 or A=A1+A2)	$\sqrt{2}$
	Form 4. (A=A1+ A3+A4)	$\frac{2}{\sqrt{3}}$

2.2. Triggering for Crack Multiple-branching in Tee Pipe Structures

In tee pipe structures under mixed-mode I/III loading, various patterns emerge among possible fracture configurations. Evidently, the actual fracture configuration may align with one of these, initiated under specific loading and geometric conditions. Multiple factors influence the crack propagation behavior, such as the crack tip geometry [27], loading mode [28-30], and the influence of a minor Mode II loading component [20].

3. Case Study Description

In an oilfield hydraulic test [5], an S32205 duplex stainless steel tee pipe (DN300×10 mm, wall thickness 10 mm, design pressure 16 MPa) burst at 22 MPa, below the target 24 MPa. Fractures initiated at the branch neck and main pipe abdomen, showing chevron patterns without plastic deformation, indicative of brittle fracture, as shown in Figure 6. Tests revealed excessive hardness (25.7-37.5 HRC, average 32.9 HRC), with -40 ℃ impact energy at 1 J and room temperature at 1-2 J, far below the standard (54 J). Metallography showed significant σ-phase at ferrite-austenite boundaries, reducing toughness. SEM identified 1 mm-long microcracks and oxide inclusions from cold forming defects. Finite element analysis confirmed stress concentration at the branch neck and main pipe abdomen. Post-verification heat treatment (1030 ℃, water cooling) increased impact energy to 258 J and reduced hardness to 200 HV, indicating improper original air cooling. Microcracks and σ-phase synergistically triggered brittle fracture in high-stress zones, well below the theoretical capacity of 43 MPa.

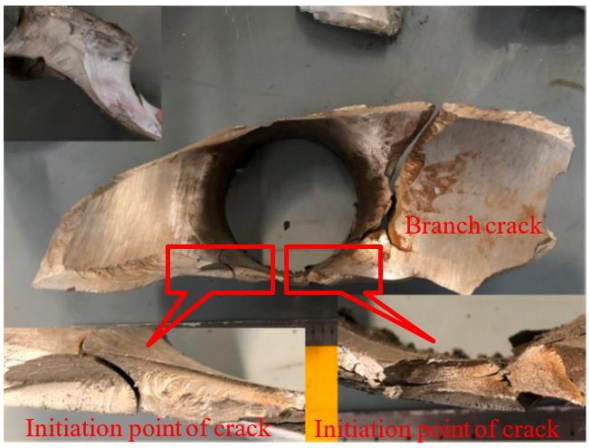

Figure 6. *Failed tee pipe junction showing crack branching and initiation site.*

4. Numerical Analysis of Tee Pipe Failure Under Mixed-Mode I/III Loading

4.1. Model Building and Meshing

As shown in Figure 7, the S32205 duplex stainless steel equal-diameter tee pipe is taken as the research object, and the length of the main pipe is 900 mm and the length of the branch pipe is 450 mm. The inner diameter of the tee pipe is 280mm, the outer diameter is 300mm, and the wall thickness is 10mm.

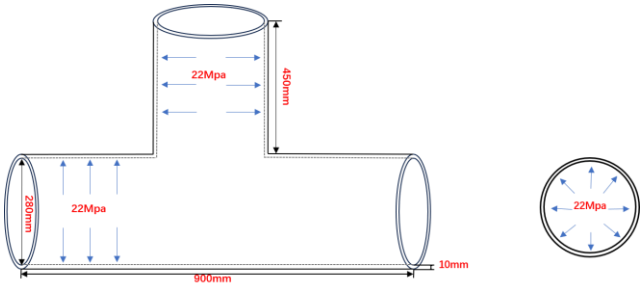

Figure 7. *Schematic diagram of the pipeline.*

During the modeling process, the main pipes and branches are generated by stretching operations and thin-walled treatments are applied to more realistically reflect the actual structure. In order to improve the mesh quality and calculation accuracy of the tee connection area, the fixed-radius mixing operation is used to model the transition of the intersection, so as to facilitate the subsequent mesh refinement and simulation analysis.

An internal pressure of 22 MPa is applied to the inside of the pipe to simulate the pressure load on the pipe under the working condition. As shown in Figure 8(a). In order to avoid the interference of the rigid body displacement on the simulation results, the two ends of the branch pipe and the main pipe are set with fixed support boundary conditions to ensure the stable force of the structure during the simulation process. As shown in Figure 8(b).

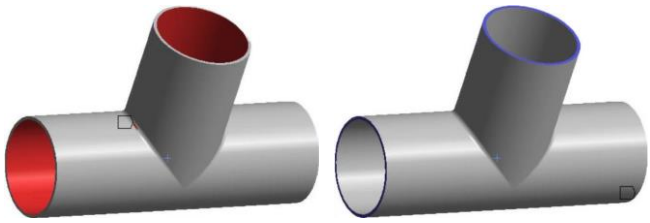

(a) Internal pressure load (b) Fixed support

Figure 8. *Pipeline internal pressure load and fixed support.*

As shown in Figure 9, the quality of the mesh is very important for finite element analysis, and this simulation is to encrypt the connection of the tee tube locally to control the size of the element and reduce the calculation error caused by the size of the mesh. For other parts of the pipeline, a loose mesh is used to divide the calculation efficiency.

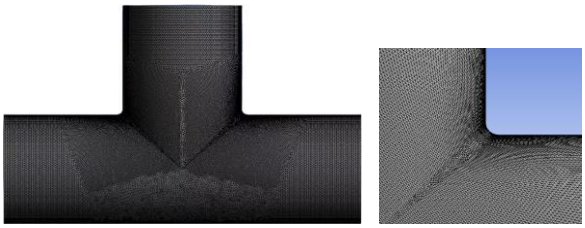

Figure 9. *Pipeline meshing.*

4.2. Stress Analysis and Defect Introduction

The numerical simulation results show that the dangerous positions in the tee tube appear on the inner surface of the neck and the outer surface of the abdomen under the action of internal pressure, and the maximum equivalent stress position is on the inner surface of the neck, so the subsequent cracks will be analyzed on the inner surface of the neck.

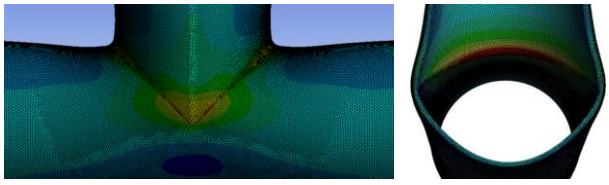

Figure 10. *Pipe equivalent stress contour.*

Semi-elliptical cracks are one of the common crack morphologies, and due to the possible displacement of both ends of the crack when loaded, it poses a potential threat to safety during pipeline operation.

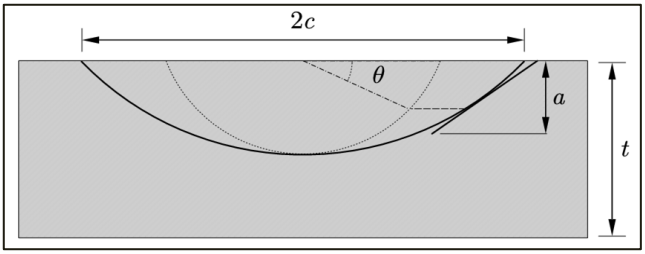

Figure 11. *Schematic Diagram of Semi-elliptical Crack*

As shown in the Figure 12, the semi-elliptical crack is inserted into the inner surface of the neck where the stress is maximum, and the crack direction is along the wall thickness.

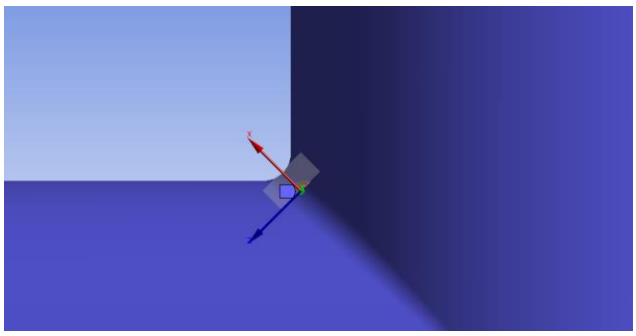

Figure 12. *Crack Insertion Location.*

In order to ensure the accuracy of the calculation, fine meshing is adopted in the crack tip area to improve the computational stability and reduce the error caused by mesh distortion or element quality problems.

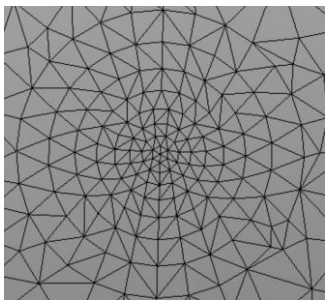

Figure 13. *Crack tip meshing.*

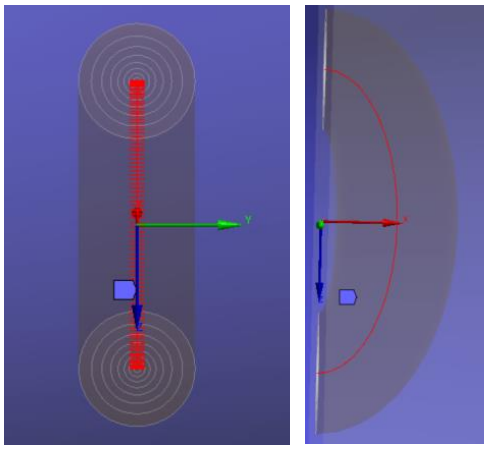

Figure 14. *Schematic Diagram of Semi-elliptical Crack.*

The crack setting is shown in the Figure 14, in order to more accurately simulate the damage mechanism of the pipeline under the action of internal pressure, the initial size parameters of the semi-elliptical crack are set to the total length of the crack 2*c*=1mm and the crack length-to-depth ratio of 0.5 at the maximum stress intensity of the pipeline, and then the crack size is analyzed by changing different crack sizes. The crack direction is set to hoop.

4.3. Grid-independent Discussions

Meshing has an important impact on the calculation accuracy of crack stress intensity factor, especially at the deepest point of crack leading edge, the degree of mesh refinement directly determines the accuracy of stress intensity factor. In order to ensure the rationality of the numerical simulation, four grid element sizes (1mm, 2mm, 3mm, 4mm, 5mm) were adjusted to evaluate the influence of the grid size on the simulation results. For four different sizes, the effects of different meshing on the type 1 crack stress intensity factor and the type 3 stress intensity factor were observed.

As shown in the Figure 15, the maximum value of the sum of the stress intensity factor does not differ significantly with the change of the grid size under different internal pressure conditions, that is, the stress intensity factor remains stable after the grid size adjustment. Therefore, in order to ensure the computational efficiency, a larger mesh size is used for the calculation in the subsequent simulations.

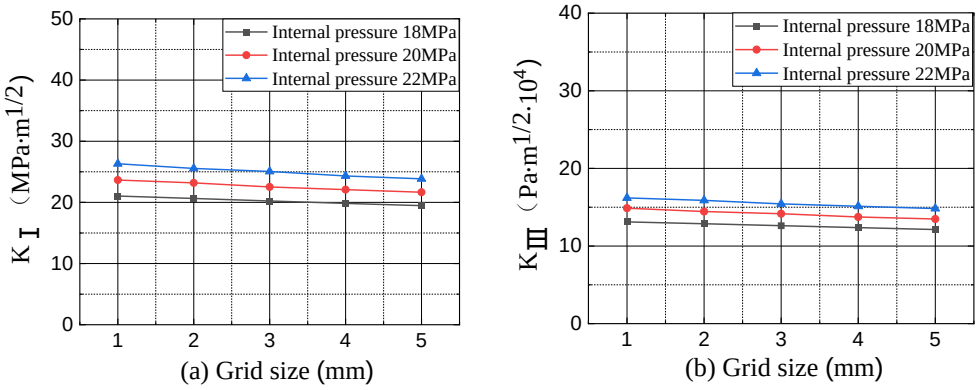

Figure 15. *Mesh independence.*

4.4. Analysis of Simulation Results

4.4.1. Under Different Internal Pressure Loads

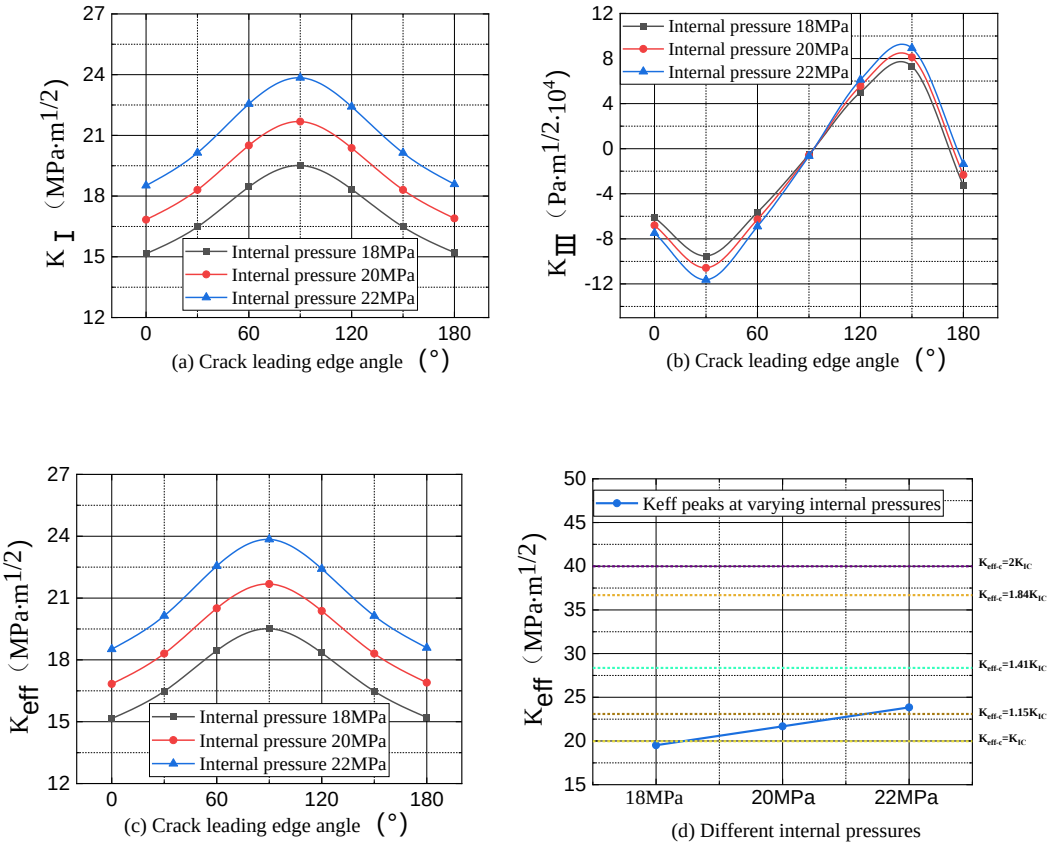

Figure 16. *Stress Intensity Factors Under Different Internal pressures.*

As shown in the Figure 16, under varying internal pressures with a crack length of 1 mm and an aspect ratio (a/c) of 0.5, the stress intensity factor K_I reaches its peak at the crack front angle of 90° (the deepest point of the crack) and gradually decreases as the angle deviates from 90°, indicating that the deepest part of the crack is dominated by opening-mode (Mode I) stress and is the core region of stress concentration. As internal pressure increases (from 18 MPa to 22 MPa), the K_I values at all angles increase significantly, with the most notable increase occurring at 90° (e.g., at 22 MPa, the K_I peak increases by approximately 20% compared to 18 MPa). This indicates that internal pressure directly in-

tensifies the opening-mode stress at the crack tip.

The K_{III} values reach local extrema near 60° and 120°. At 18 MPa, K_{III} remains positive (indicating outward tearing stress), while at 20 MPa and 22 MPa, negative values appear at certain angles (indicating inward tearing stress), suggesting that internal pressure variations may alter the direction of shear stress at the crack front. As internal pressure increases, the absolute values of K_{III} also increase, though the distribution range of positive and negative values changes only slightly. This indicates that internal pressure mainly affects the magnitude of the tearing-mode stress rather than its direction. The stress concentration at 60° and 120° shows that the crack surface edges are primarily subjected to shear forces.

K_{eff} reaches its maximum value at 90°, consistent with the dominant effect of Mode I stress intensity. However, the K_{eff} values are higher than the corresponding K_I values, reflecting the coupling effect between Mode I and Mode III stresses (e.g., at 22 MPa, the K_{eff} peak is approximately 10% higher than K_I under the same conditions).

K_{eff} increases linearly with internal pressure. At 22 MPa, the K_{eff} peak approaches the material's fracture toughness, indicating that under high internal pressure, the crack is already in a critical state of unstable propagation.

In summary, internal pressure is a key factor affecting stress intensity factors. It intensifies stress concentration at the crack tip by increasing both opening-mode (Mode I) and tearing-mode (Mode III) stresses, with the most significant impact observed at the deepest point of the crack (90°).

The growth rate of the equivalent stress intensity factor (K_{eff}) is greater than that of Mode I alone, suggesting that crack propagation under internal pressure is governed by multi-mode stress coupling. Therefore, three-dimensional fracture criteria such as the Richard criterion should be used for accurate safety assessment.

According to Figure 16(d) $K_{eff-C} = 20\text{MPa}\cdot\text{m}^{1/2}$, the following observations can be made:

When the internal pressure is 20 MPa, $K_{eff-C} \geq K_{I-C}$ crack extension Form 1 (A = A1 + A2 + A3 + A4), as listed in Table 1, may be triggered.

When the internal pressure increases to 22 MPa, $K_{eff-C} \geq \frac{2}{\sqrt{3}} K_{I-C}$ both crack extension Form 1 (A = A1 + A2 + A3 + A4) and Form 4 (A = A1 + A3 + A4) may be triggered.

4.4.2. Different Half-length-to-depth Ratios

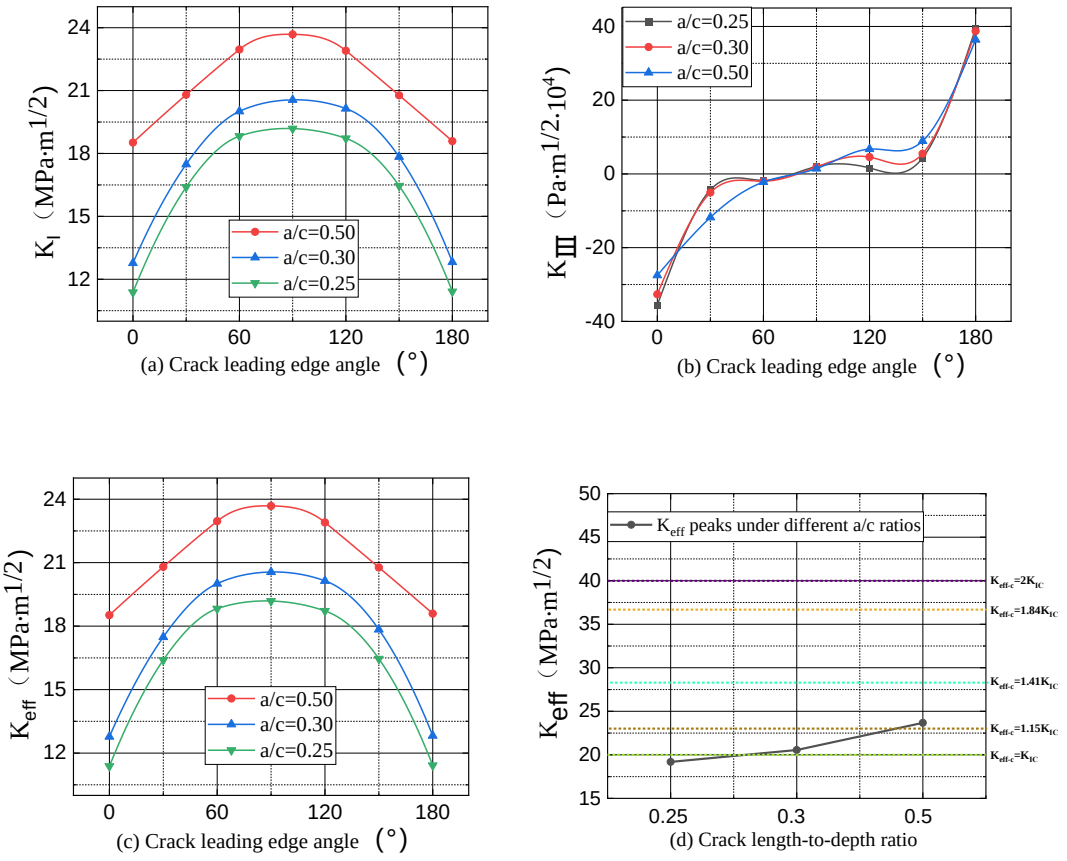

Figure 17. *Stress Intensity Factors Under Varying Crack Aspect Ratios (a/c).*

As shown in the Figure 17, the internal pressure is 22MPa, and the crack length is 1mm, the K_I curves for different aspect ratios a/c (0.25, 0.30, 0.50) all reach their peak values at the 90 ° position, and these peak values increase significantly with increasing a/c (approximately 24 for a/c = 0.50 compared to about 15 for a/c = 0.25). This indicates that Mode I stress is the primary factor governing crack propagation, with Mode I cracks driven by tensile stress predominating in the central region of the pipe. The curves demonstrate stronger symmetry, with K_I values approaching zero at 0 ° and 180 °, suggesting that the crack surface ends are mainly subjected to shear and tearing stresses rather than tensile opening stress.

The peak of K_{III} appears at 60 ° and 120 °, instead of 90 °, indicating that the central region of the crack front is primarily affected by tearing (Mode III) stress. The region with the maximum shear stress corresponds to the concentration of Mode III stress around 60 °. As the a/c ratio increases, the absolute value of K_{III} also rises (e.g., about 40 for a/c = 0.50 compared to approximately 20 for a/c = 0.25), indicating that a higher aspect ratio intensifies the concentration of tearing stress. However, the overall magnitude remains lower than that of Mode I stress, confirming that Mode I is dominant and the influence of Mode III is relatively limited. The curves are symmetric about 90 °, with values at 60 ° and 120 ° having equal magnitudes and opposite signs, reflecting that the tearing stresses on both sides of the crack front act in opposite directions—consistent with stress distribution under torsional loading in mechanics of materials.

The K_{eff} distribution is similar to that of K_I. For all aspect ratios a/c (0.25, 0.30, 0.50), the curves reach their peak at 90 °, indicating that the equivalent stress concentration is most severe at the deepest point of the crack. As a/c increases, the peak value of K_{eff} also rises markedly (approximately 24 for a/c = 0.50, significantly higher than 15 for a/c = 0.25), suggesting that the greater the aspect ratio, the higher the overall stress intensity at the crack tip, making unstable crack propagation more likely. The curves are generally symmetric (with similar values at 0 ° and 180 °), indicating that the stress states at the crack surface ends are similar. Nevertheless, the stress concentration peaks in the depth direction, implying that crack propagation predominantly occurs through the thickness.

Compared with Figure 17(a), the peak trend of K_{eff} closely follows that of K_I, further confirming that Mode I stress makes the largest contribution to the comprehensive fracture criterion. However, accurate crack behavior assessment still requires incorporating the effects of both Mode II and Mode III stresses.

Overall, all three stress intensity factors (K_I, K_{III}, and K_{eff}) increase with increasing a/c, indicating that deeper cracks (relative to their half-length) lead to more pronounced stress concentration at the crack tip and are more susceptible to unstable propagation. The peak values of K_{eff} and K_I occur at the deepest point of the crack (90 °), marking it as the critical region for fracture. In contrast, the peak of K_{III} appears at 60 °/120 °, reflecting the localized nature of tearing stress concentration.

Under the condition that the internal pressure is 22MPa and the crack length-to-depth ratio is 0.5, the crack length is changed. The stress intensity factor K_I reaches its maximum at the crack front angle of 90 ° (the deepest point of the crack) and gradually decreases as the angle deviates from 90 °, indicating that the deepest point of the crack is dominated by opening-mode (Mode I) stress. This suggests that the depth direction of the crack is the core region of Mode I stress concentration. As the half-length of the crack, c, increases (from 0.5 mm to 2.0 mm), the values of K_I at all angles increase significantly, with the most pronounced increase at 90 ° (e.g., when c = 2.0 mm, the K_I peak increases by approximately 50% compared to c = 0.5 mm). This reflects the direct influence of crack size on the opening-mode stress intensity factor: the deeper the crack, the more pronounced the tip stress concentration. An increasing a/c ratio leads to a higher stress intensity factor.

According to Figure 17(d) $K_{eff-C} = 20\text{MPa}\cdot\text{m}^{1/2}$, the following observations can be made:

When the aspect ratio a/c is 0.3, $K_{eff-C} \geq K_{\text{I}-C}$ crack extension Form 1 (A = A1 + A2 + A3 + A4), as listed in Table 1, may be triggered.

When the aspect ratio increases to 0.5, $K_{eff-C} \geq \frac{2}{\sqrt{3}} K_{\text{I}-C}$ both crack extension Form 1 (A = A1 + A2 + A3 + A4) and Form 4 (A = A1 + A3 + A4) may be triggered.

4.4.3. Different Crack Half-length

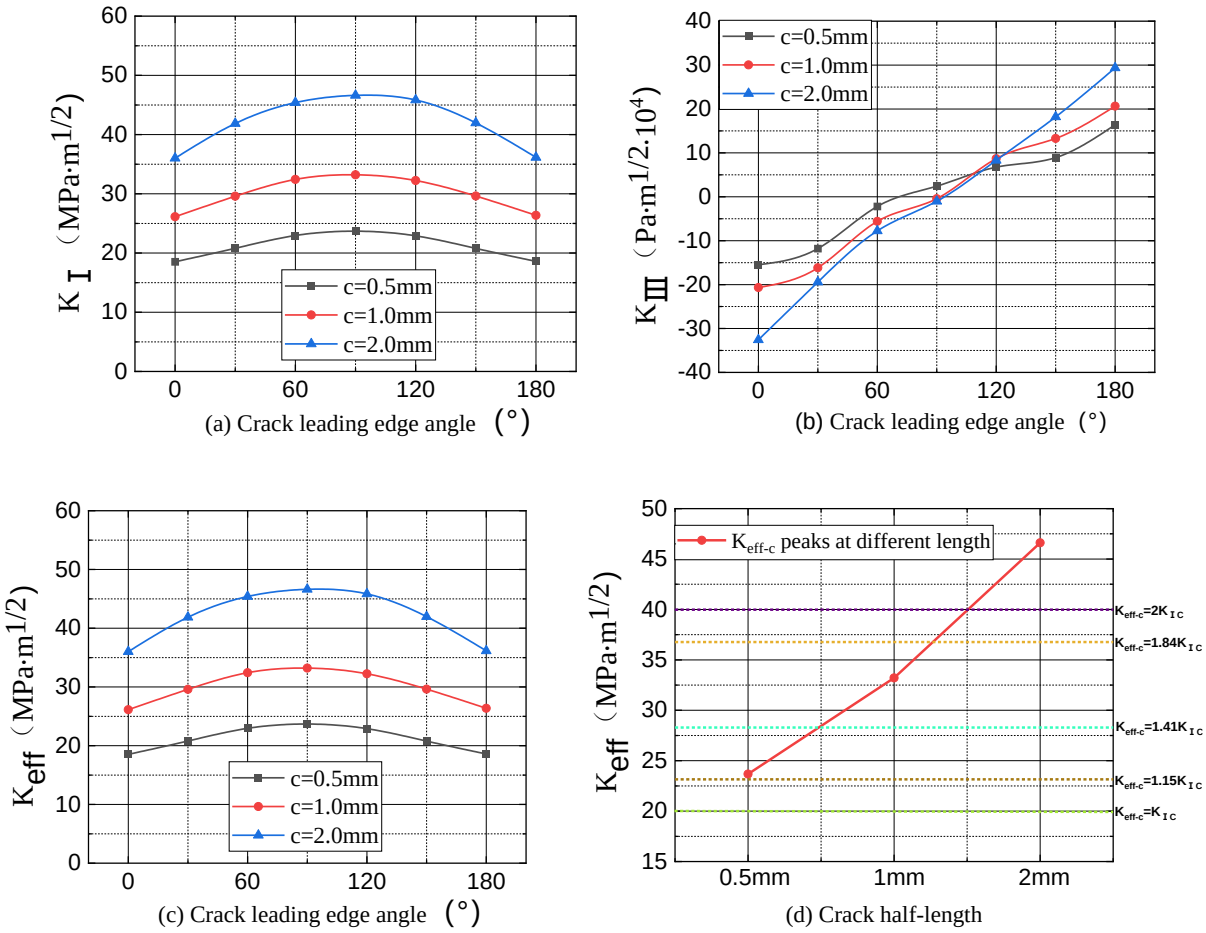

Figure 18. *Stress Intensity Factors Under Varying Crack Half-Lengths (c).*

As shown in the Figure 18, Under the condition that the internal pressure is 22MPa and the crack length-to-depth ratio is 0.5, the crack length is changed. The stress intensity factor K_I reaches its maximum at the crack front angle of 90° (the deepest point of the crack) and gradually decreases as the angle deviates from 90° , indicating that the deepest point of the crack is dominated by opening-mode (Mode I) stress. This suggests that the depth direction of the crack is the core region of Mode I stress concentration. As the half-length of the crack, c, increases (from 0.5 mm to 2.0 mm), the values of K_I at all angles increase significantly, with the most pronounced increase at 90° (e.g., when c = 2.0 mm, the K_I peak increases by approximately 50% compared to c = 0.5 mm). This reflects the direct influence of crack size on the opening-mode stress intensity factor: the deeper the crack, the more pronounced the tip stress concentration. An increasing a/c ratio leads to a higher stress intensity factor.

The K_{III} values reach local extrema near 60° and 120° . When c = 0.5 mm, K_{III} remains positive (indicating outward-directed tearing stress), while at $c \geqslant$ 1.0 mm, negative values appear at certain angles (indicating inward-directed tearing stress), demonstrating that crack half-length influences the direction of shear stress. As c increases, the absolute values of K_{III} increase overall particularly at 60° and 120° indicating that tearing-mode stresses at the crack edges intensify with crack growth. The appearance of negative K_{III} values suggests that larger cracks may induce reverse shear stress, exacerbating torsional deformation along the crack surface.

The equivalent stress intensity factor K_{eff} reaches its maximum at 90° and increases significantly with larger c values (e.g., when c = 2.0 mm, the K_{eff} peak increases by approximately 40% compared to c = 0.5 mm), reflecting the combined influence of Mode I and Mode III stresses. The K_{eff} values exceed those of K_I alone, indicating that mixed-mode fracture criteria must account for the coupling of different crack modes. When c = 2.0 mm, K_{eff} near 90° approaches or surpasses the material's fracture toughness, suggesting that deep cracks are more likely to satisfy the conditions for unstable propagation under sliding loads. In contrast, relying solely on K_I may underestimate the risk (e.g., K_I may remain

below the critical value while K_{eff} exceeds it).

In summary, increasing the crack half-length c significantly elevates the Mode I, Mode III, and equivalent stress intensity factors. Among them, the concentration of Mode I stress at the crack's deepest point (90 °) is most pronounced, making it the primary driving force for crack propagation in the thickness direction.

According to Figure 18(d) $K_{eff-C} = 20\text{MPa}\cdot\text{m}^{1/2}$ When the crack half-length is 0.5mm, $K_{eff-C} \geq \frac{2}{\sqrt{3}} K_{\text{I}-C}$ crack extension Form 1 (A = A1 + A2 + A3 + A4) and Form 4 (A = A1 + A3 + A4), as listed in Table 1, may be triggered.

When the crack half-length is 1 mm, $K_{eff-C} \geq \sqrt{2} K_{\text{I}-C}$ crack extension Forms 1 (A = A1 + A2 + A3 + A4), 4 (A = A1 + A3 + A4), and 3 (A = A1 + A4 or A = A1 + A2) may be triggered.

When the crack half-length is 2 mm, $K_{eff-C} \geq 2K_{\text{I}-C}$ all possible crack extension configurations listed in Table 1 may be triggered.

5. Discussion

The finite element analysis of the S32205 duplex stainless steel tee pipe under mixed-mode I/III loading provides critical insights into crack propagation behavior and fracture mechanisms. The results from Figures 16-18 indicate that crack extension configurations, as outlined in Table 1, are highly sensitive to internal pressure, crack geometry, and crack size. At an internal pressure of 20 MPa, the crack extension Form 1 (A=A1+A2+A3+A4) is likely to initiate, while at 22 MPa, both Form 1 and Form 4 (A=A1+A3+A4) may be triggered. Similarly, with a crack depth-to-length ratio (a/c) of 0.3, Form 1 is predominant, but at a/c = 0.5, both Form 1 and Form 4 become viable. For crack half-lengths (c), a value of 0.5 mm activates Form 1 and Form 4, whereas c = 1 mm additionally triggers Form 3 (A=A1+A4 or A=A1+A2). At c = 2 mm, all fracture propagation modes in Table 1, including tri-branching and side-branching, are potentially activated, reflecting the heightened instability of deeper cracks. This trend aligns with the observed increase in the effective stress intensity factor K_{eff-C}, which peaks at the crack's deepest point (90 °) and escalates with larger a/c and c values, indicating a greater propensity for unstable crack growth.

Several factors further exacerbate this behavior. Improper heat treatment, corrosion, loading mode, and the influence of a minor Mode II loading component jointly reduce the fracture toughness of the tee pipe. The precipitation of σ-phase from improper air-cooling induces material embrittlement, while corrosion-driven imperfections amplify crack nucleation. Mixed-mode I/III loading elevates K_{eff-C}, and a minor Mode II contribution further alters crack propagation trajectories, fostering brittle fracture in vulnerable zones such as the branch neck. This interplay introduces uncertainty in triggering various fracture propagation modes, as evidenced by the diverse configurations activated under different conditions.

The simulated high-stress regions at the branch neck and main pipe abdomen corroborate experimental observations of chevron patterns, validating the energy-based model's predictive reliability. However, discrepancies may arise due to unmodeled factors like notch geometry or dynamic loading effects. Future studies should explore these aspects to enhance the model's applicability, particularly under cyclic or impulse loading conditions prevalent in oilfield operations, and investigate strategies to mitigate material defects through advanced manufacturing techniques.

6. Conclusions

This study successfully demonstrates the efficacy of an energy-based model in elucidating the brittle fracture characteristics of an S32205 duplex stainless steel tee pipe under mixed-mode I/III loading. The analysis reveals that Mode I stresses predominantly govern crack propagation at the deepest crack front, while Mode III contributions induce localized tearing, with the effective stress intensity factor K_{eff-C} escalating with increasing crack depth and length. High-stress zones, notably the branch neck and main pipe abdomen, are identified as critical sites for crack initiation, aligning with experimental observations of chevron patterns. The study underscores the pivotal role of metallurgical imperfections, including σ-phase precipitation from improper heat treatment and corrosion-induced defects, in reducing fracture toughness and accelerating brittle failure. These findings affirm the model's predictive accuracy in capturing complex fracture behaviors. To enhance structural reliability in oilfield applications, the adoption of optimized heat treatment protocols, such as water cooling at 1030 ℃, and the implementation of ultrasonic testing to detect micro-cracks are recommended. These measures offer practical pathways to mitigate tee pipe vulnerabilities, ensuring safer operation of high-pressure oil and gas pipelines.

Future research should focus on extending the energy-based model to account for dynamic loading conditions, such as impulse or cyclic pressures, which are prevalent in oilfield operations and may alter crack propagation dynamics. Additionally, investigating the influence of notch geometry and surface imperfections on mixed-mode fracture behavior could further refine the model's applicability to complex tee pipe configurations. From a practical perspective, implementing advanced manufacturing protocols, such as controlled heat treatment processes at 1030 ℃ with water cooling, is recommended to eliminate σ-phase formation and enhance material toughness. Routine ultrasonic testing should be integrated into quality control procedures to detect micro-cracks early, particularly in cold-formed components. These measures, combined with in-field metallographic and

hardness assessments, can significantly improve the reliability of tee pipe junctions, reducing the likelihood of catastrophic failures in high-pressure oil and gas pipelines.

Abbreviations

α_i	Angle Between the Shifting Direction of the Local Boundary and x_i -axis and Its Critical Value
n_i	The Unit Normal Vector of the Boundary
η	Configuration-dependent Fracture Toughness Amplification Factor
c	Crack Half-length
a	Crack Depth
ϕ	Normalized Mode Mixity Angle
μ	Poisson's Ratio
σ_{ij}	Stress Components
A, A_i	Boundary Surfaces or Integration Paths Around the Crack Tip
E	Young's Modulus
G	Energy Release Rate for Boundary Shifting
$\Gamma(\varphi)$	Normalized Energy-driven Parameter
J_i	Conservation Integrals
K_{eff}	The Effective Stress Intensity Factor
K_{eff-C}	K-based Effective Fracture Toughness
K_{IC}	Fracture Toughness for Pure Mode-I Crack Extension
K_I K_{III}	Stress Intensity Factors for the Mode-I or Mode-III Deformations
r_o	Polar Coordinate of the Boundary Surface Around Crack Tip

Conflicts of Interest

The authors declare no conflicts of interest.

References

[1] Xie, Z., Jin, Q., Su, G., & Lu, W. (2024). A Review of Hydrogen Storage and Transportation: Progresses and Challenges. Energies, 17(16), 4070. https://doi.org/10.3390/en17164070

[2] Cao, J., Ma, W., Pang, G., Wang, K., Ren, J., Nie, H.,... & Yao, T. (2021). Failure analysis on girth weld cracking of underground tee pipe. International Journal of Pressure Vessels and Piping, 191, 104371. https://doi.org/10.1016/j.ijpvp.2021.104371

[3] Ashrafizadeh, H., Karimi, M., & Ashrafizadeh, F. (2013). Failure analysis of a high pressure natural gas pipe under split tee by computer simulations and metallurgical assessment. Engineering Failure Analysis, 32, 188-201. https://doi.org/10.1016/j.engfailanal.2013.03.013

[4] Ahmed, F., Ali, L., Iqbal, J., & Hasan, F. (2008). Failure of pipe joints during hydrostatic testing. Engineering Failure Analysis, 15(6), 766-773. https://doi.org/10.1016/j.engfailanal.2007.06.008

[5] Zhang, S. (2020). Failure analysis on tee pipe of duplex stainless in an oilfield. Engineering Failure Analysis, 115, 104676. https://doi.org/10.1016/j.engfailanal.2020.104676

[6] Wang, L., Xie, Y. J., & Yuan, H. (2023). Potential fracture configurations of a cracked solid under mixed mode-I/III loading. Archive of Applied Mechanics, 93(5), 2033-2049. https://doi.org/10.1007/s00419-023-02371-x

[7] M. R. M Aliha, M. R. Ayatollahi. Analysis of fracture initiation angle in some cracked ceramics using the generalized maximum tangential stress criterion. Int. J. Solids Struct. 49(2012) 1877-83.https://doi.org/10.1016/j.ijsolstr.2012.03.029

[8] F. Erdogan, G. C. Sih. On the crack extension in plates under plane loading and transverse shear. J. Basic Eng. Trans ASME. 85(1963) 519-25.

[9] G. C. Sih. Strain-energy-density factor applied to mixed Mode crack problems. Int. J. Fract. 10(1974) 305-21.

[10] M. A. Hussain, S. L. Pu, J. Underwood. Strain energy release rate for a crack under combined Mode I and Mode II. Fracture Analysis, 1974. ASTM STP 560. American Society for Testing and Materials, Philadelphia, pp. 2–28.

[11] J. Akbardoost, M. R. Ayatollahi, M. R. M Aliha, M. J. Pavier, D. J. Smith. Size-dependent fracture behavior of Guiting limestone under mixed Mode loading. Int. J. Rock Mech. Min. Sci. 71(2014) 369-80. https://doi.org/10.1016/j.ijrmms.2014.07.019

[12] M. R. M. Aliha, Gh. R. Hosseinpour, M. R. Ayatollahi. Application of cracked triangular specimen subjected to three-point bending for investigating fracture behavior of rock materials. Rock Mech. Rock Eng. 46(2013) 1023–34. https://doi.org/10.1007/s00603-012-0325-z

[13] M. M. Mirsayar, A. Razmi, M. R. M Aliha, F. Berto. EMTSN criterion for evaluating mixed mode I/II crack propagation in rock materials. Eng. Fract. Mech. 190(2018): 186-97. https://doi.org/10.1016/j.engfracmech.2017.12.014

[14] M. R. M Aliha, F. Berto, A. Mousavi, S. M. J. Razavi. On the applicability of ASED criterion for predicting mixed mode I+II fracture toughness results of a rock material. Theor. Appl. Fract. Mech. 92(2017) 198-204. https://doi.org/10.1016/j.tafmec.2017.07.022

[15] S. M. J. Razavi, M. R. M. Aliha, F. Berto. Application of an average strain energy density criterion to obtain the mixed mode fracture load of granite rock tested with the cracked asymmetric four-point bend specimens. Theor. Appl. Fract. Mech. 97(2018) 419-25. https://doi.org/10.1016/j.tafmec.2017.07.004

[16] B. Cotterell, J. R. Rice. Slightly curved or kinked cracks. Int. J. Fract. 16(1980) 155-69.

[17] B. Lin, M. E. Mear, K. Ravi-Chandar. Criterion for initiation of cracks under mixed-mode I+III loading. Int J Fract. 165 (2010) 175–188. https://doi.org/10.1007/s10704-010-9476-7

[18] X. H. Li, X. Y. Zheng, W. J. Yuan, X. W. Cui, Y. J. Xie, Y. Wang. Instability of cracks initiation from a mixed-mode crack tip with iso-stress intensity factors KI and KII. Theor. Appl. Fract. Mech. 96(2018) 262-71. https://doi.org/10.1016/j.tafmec.2018.05.004

[19] Y. J. Xie, J. Li, X. Z. Hu, X. H. Wang, Y. M. Cai, W. Wang. Modelling of multiple crack-branching from Mode-I crack-tip in isotropic solids. Eng. Fract. Mech. 109(2013) 105-16. https://doi.org/10.1016/j.engfracmech.2013.01.009

[20] Y. J. Xie, Y. L. Duo, H. Yuan. Potential fracture paths for cracked rocks under compressive-shear loading. Int. J. Rock Mech. Min. Sci. 128(2020) 104216. https://doi.org/10.1016/j.ijrmms.2020.104216

[21] H. Yuan, Y. J. Xie, W. Wang. Underlying fracture trends on Mode-I crack multiple-branching. Eng. Fract. Mech. 225(2020) 106835. https://doi.org/10.1016/j.engfracmech.2019.106835

[22] J. Li, Y. J. Xie, X. Y. Zheng, Y. M. Cai. Underlying fracture trends and triggering on Mode-II crack branching and kinking for quasi-brittle solids. Eng. Fract. Mech. 211(2019) 382–400. https://doi.org/10.1016/j.engfracmech.2019.02.036

[23] J. D. Eshelby. The Force on an Elastic Singularity. Phil. Trans. Roy. Soc. London Ser A. 244(1951) 87-112.

[24] B. Budiansky and J. R. Rice. Conservation Laws and Energy-Release Rates. ASME J. Appl. Mech. 40(1973) 201-203.

[25] A. A. Griffith. The Phenomena of Rupture and Flow in Solids. Phil. Trans. Roy. Soc. Lon. Ser. A. 221(1921) 163-198.

[26] G. P. Cherepanov. Mechanics of Brittle Fracture, Moscow, Publish House "Nuaka," 1974, English translation published by McGraw-Hill International Book Co., New York; 1979: 266-69.

[27] V. Hakim, A. Karma. Crack path prediction in anisotropic brittle materials. Phys. Rev. Lett. 95 (2005) 235501. https://doi.org/10.1103/PhysRevLett.95.235501

[28] A. Karma, D. A. Kessler, H. Levine. Phase-field model of mode III dynamic fracture. Phys. Rev. Lett. 87 (2001) 045501. https://doi.org/10.1103/PhysRevLett.87.045501

[29] K. Ravi-Chandar, W. G. Knauss. An experimental investigation into dynamic fracture: III. On steady-state crack propagation and crack branching. International Journal of Fracture. 26 (1984) 141-154.

[30] M. R. M. Aliha, E. Linul, A. Bahmani, L. Marsavina. Experimental and theoretical fracture toughness investigation of PUR foams under mixed mode I+III loading. Polymer Testing. 67(2018) 75-83. https://doi.org/10.1016/j.polymertesting.2018.02.015